SI APPENDIX

Supplementary Figures 1-12

Supplementary Table 1

A

Superkingdom	All RtcB	RtcB2
Bacteria	16,044	1,437
Archaea	1,876	0
Eukaryota	1,049	98
Viruses	241	1

B

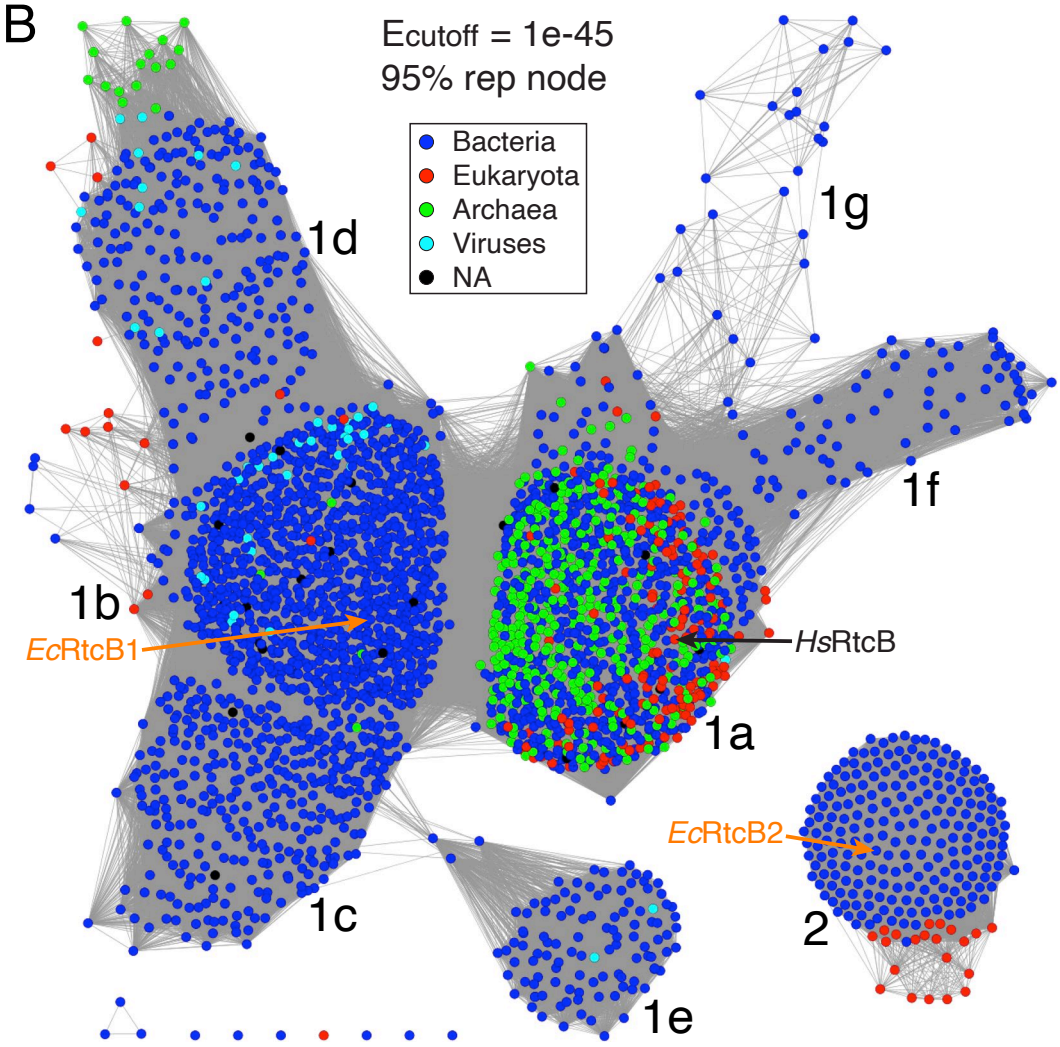

Figure S1. Bioinformatic analysis of RtcB. (*A*) The numbers of unique sequences of RtcB found in three superkingdoms of life and viruses. (*B*) Sequence Similarity Network (SSN) of RtcB. See Materials and Methods for details of constructing the network. Notably, this SSN was generated using only 25% of sequences on the database. Each node (colored cycle) represents a collection of RtcB sharing >95% sequence identity (95% rep node). An edge (gray line) connects two nodes if the E-value measuring their sequence similarities is smaller than the cutoff value (1e-45 for this network). The entire SSN has been arbitrarily divided into 8 clusters (1a-g, and 2). The nodes representing two *E. coli* RtcB are marked with orange arrows, and the node representing human RtcB (*Hs*RtcB) is also marked with a black arrow for comparison.

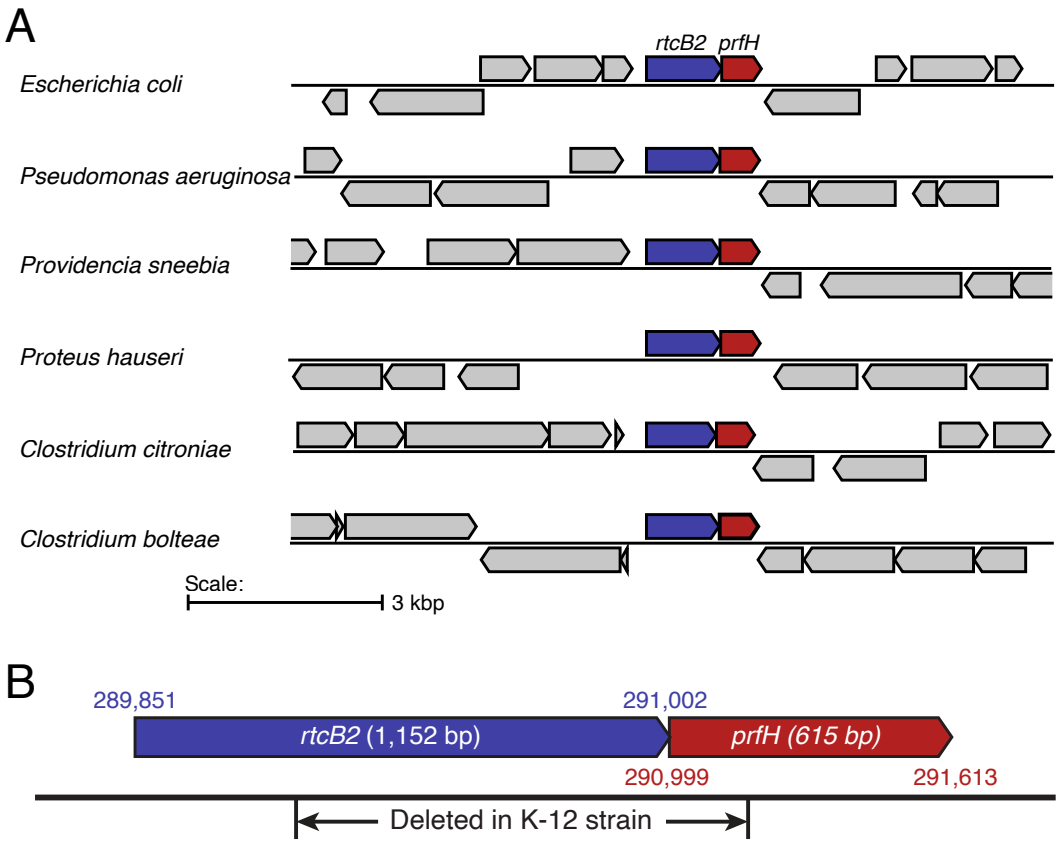

Figure S2. The genes encoding bacterial RtcB2 and PrfH are predominately found in a two-component operon. (*A*) Six representatives of genomic organizations centered at the *rtcB2-prfH* operon. The genes encoding RtcB2 and PrfH are highlighted in colored boxes. (*B*) Close-up view of the operon encoding *E. coli* RtcB2 and PrfH. *Ec*RtcB2 and *Ec*PrfH are co-translational, demonstrated by the overlap of the stop codon for RtcB2 and the start codon for PrfH. All *E. coli* strains encode full-length RtcB2 and PrfH except for K-12 strain and its derivatives, which have a large genomic deletion that encompasses the coding regions of both proteins.

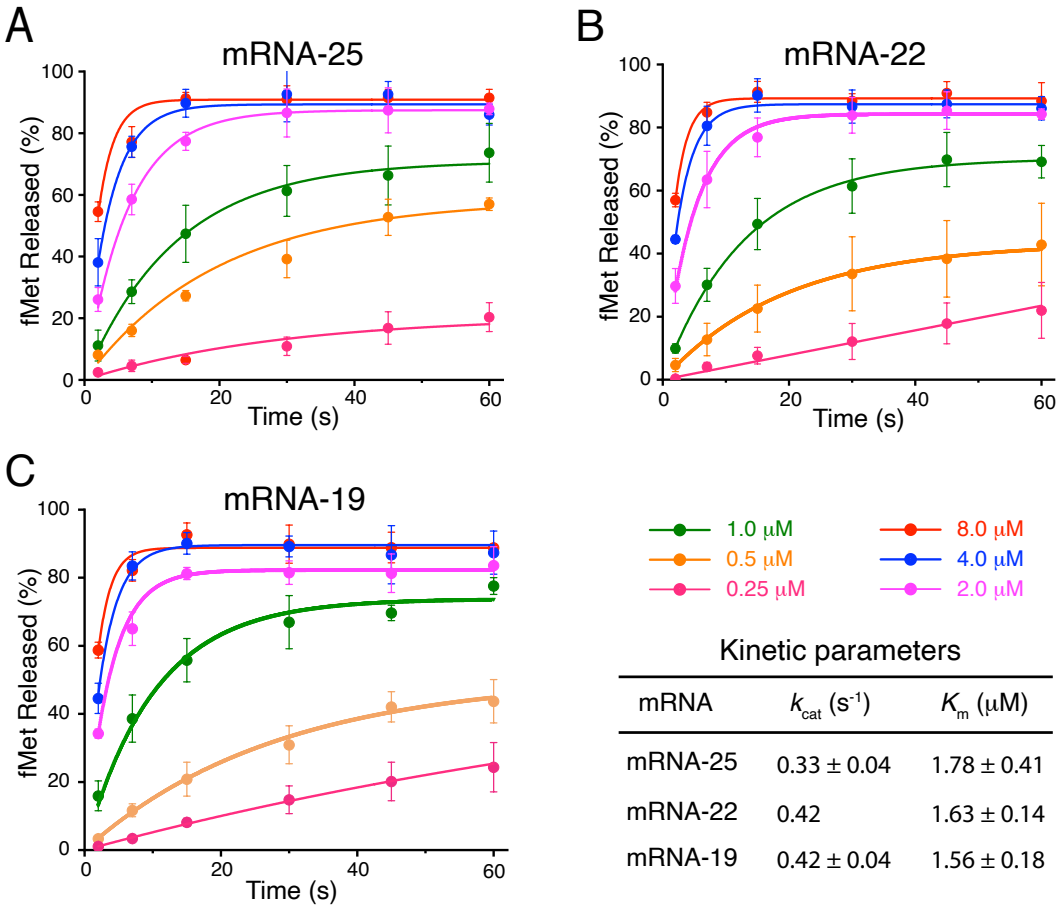

Kinetic parameters

mRNA	k_{cat} (s^{-1})	K_m (μM)
mRNA-25	0.33 ± 0.04	1.78 ± 0.41
mRNA-22	0.42	1.63 ± 0.14
mRNA-19	0.42 ± 0.04	1.56 ± 0.18

Figure S3. Expanded peptide release assays with *Ec*PrfH. (*A-C*) Time course of the peptide release assays using various concentrations of *Ec*PrfH. Each experiment was repeated three times, and the same assays were carried out for three different mRNAs listed in Fig. 1*A*. These assays allowed us to obtain kinetic parameters listed in the table.

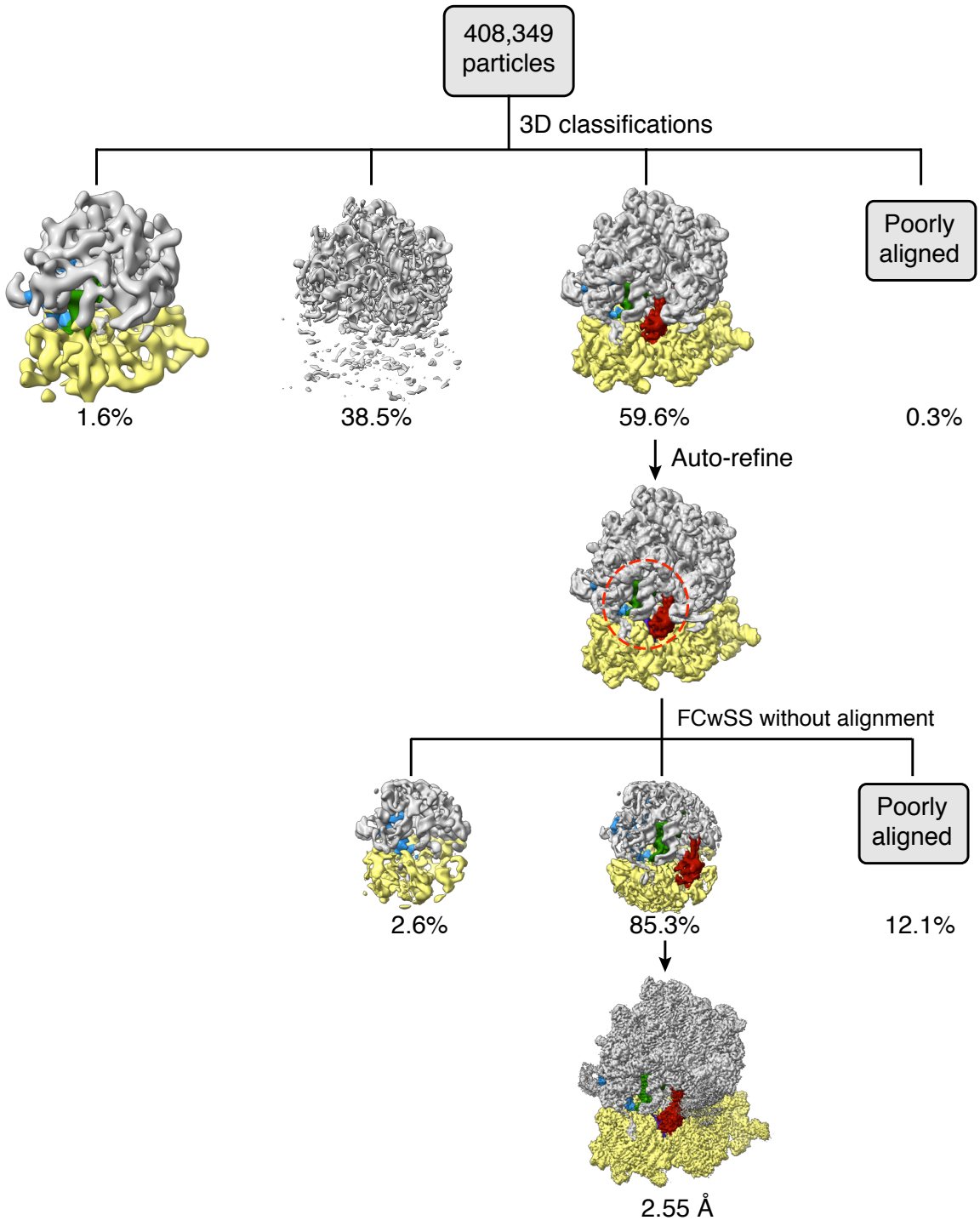

Figure S4. Cryo-EM classification of *Ec*PrfH in complex with the damaged *E. coli* 70S ribosome. The complete dataset of 408,349 particles was initially classified in four classes. The resulting class 2 (243,376 particles) was further refined and subject to focused classification with signal subtraction (FCwSS) in Relion. The remaining 207,600 particles that contain PrfH were then 3D-refined, resulting in a final reconstruction of 2.55 Å average resolution.

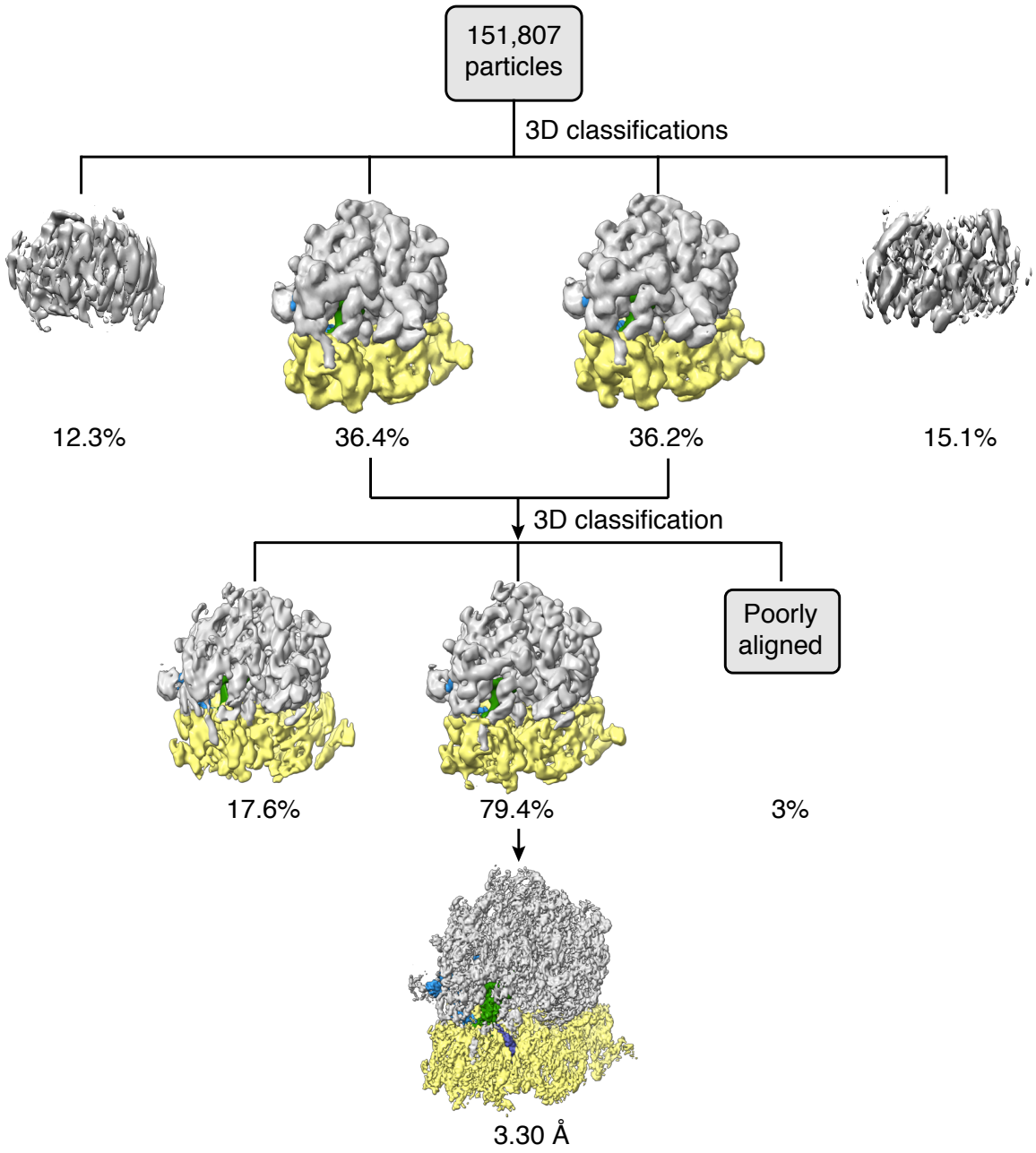

Figure S5. *Ec*PrfH is not found in the intact 70S complex. Cryo-EM classification of *Ec*PrfH in complex with the intact *E. coli* 70S ribosome. 151,807 particles selected from 2D classification were classified by two rounds of 3D classifications in Relion to removing the subunits and poorly aligning particles. The final reconstruction with P- and E-tRNA in the ribosome has a nominal resolution of 3.3 Å.

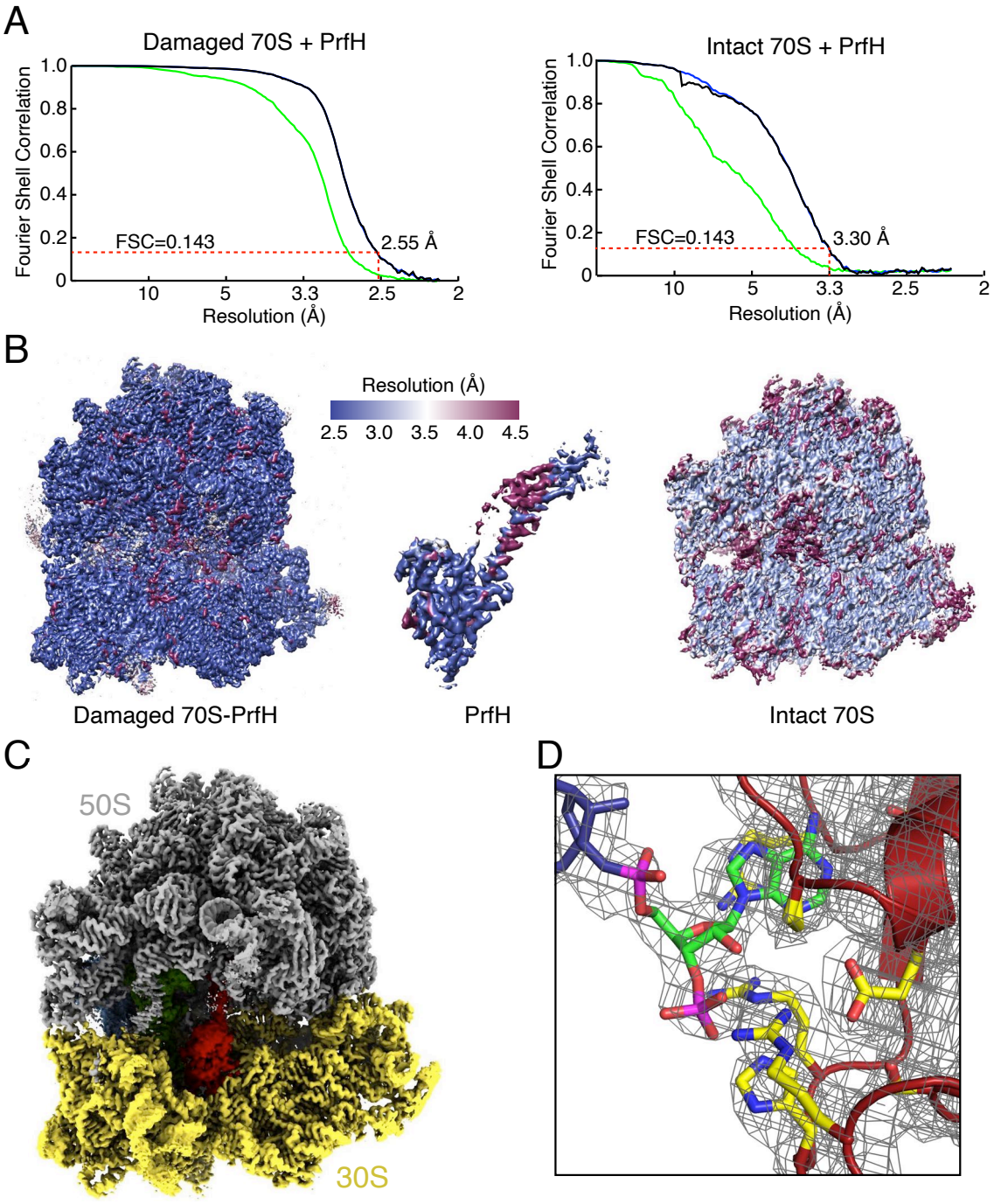

Figure S6. Cryo-EM resolution and map. (*A*) Gold-standard FSC curves for the electron microscopy map of damaged 70S ribosome (left panel) and intact 70S ribosome (right panel). Resolution is demarcated using the FSC=0.143 criterion. (*B*) Unfiltered and unsharpened density map colored by local resolution in surface for the damaged 70S ribosome, PrfH, and the intact 70S ribosome. (*C*) Cryo-EM density map of the damaged 70S•PrfH•tRNA•mRNA complex. The complex is oriented and colored the same as the structure shown in Fig. 2*A*. (*D*) Cryo-EM density map highlighting the structure of A1493P. The structures are depicted the same as in Fig. 3*B* except for omission of hydrogen bonding and addition of cryo-EM density map contoured at 2.0 σ.

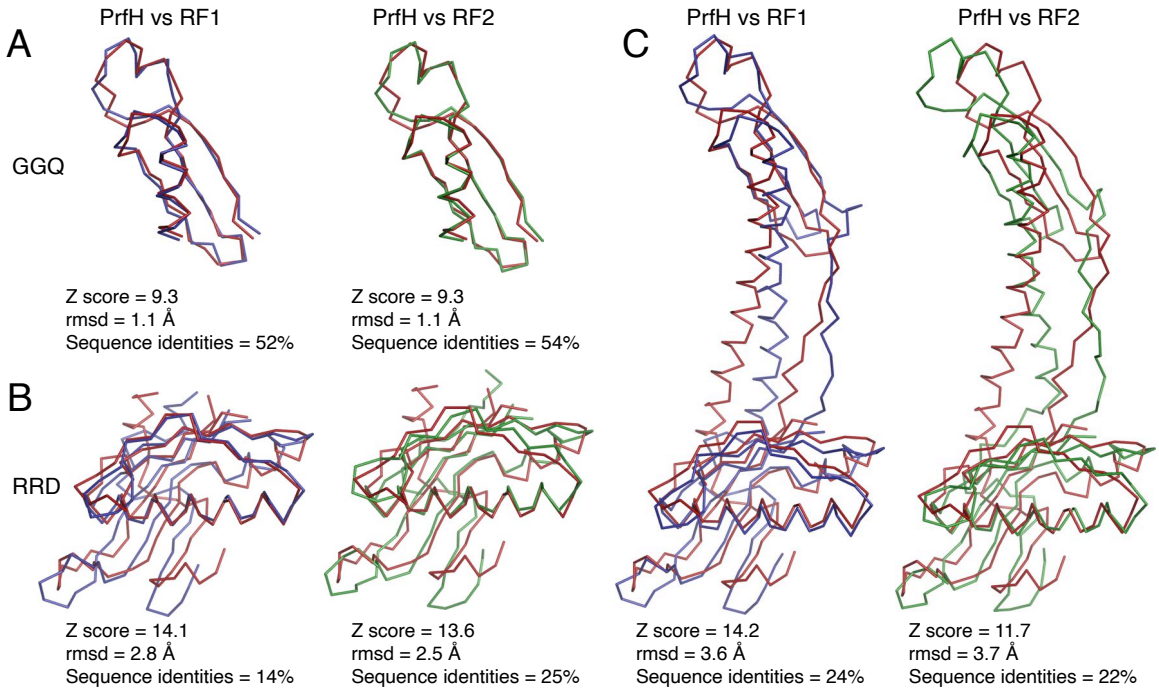

Figure S7. Structural alignments of *Ec*PrfH with their counterparts from RF1 and RF2. (*A*-*B*) Structural alignments of the individual domains. (*C*) Structural alignments of the full-length protein. The pairwise structural comparisons were carried out at Dali server (http://ekhidna2.biocenter.helsinki.fi/dali/). The Z score of Dali search as well as rmsd of three structures are listed. The pairwise sequence alignments were carried out using Blastp at NCBI, and the percentiles of sequence identities are also listed. PrfH is colored red, RF1 is in blue, and RF2 is in green.

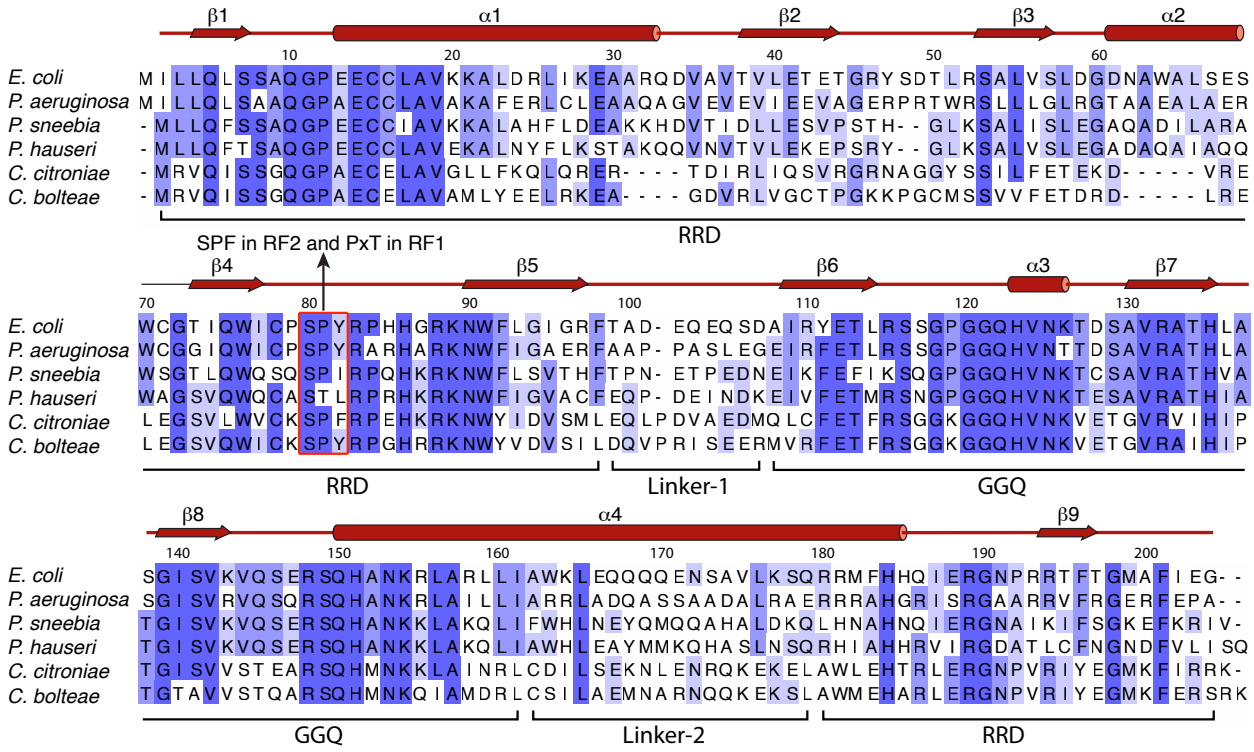

Figure S8. Secondary structure and domain boundaries of PrfH. PrfH sequences from six organisms shown in Fig. S2*A* were aligned. The conservation was colored by different shades of blue. The numbers on the top of the sequences correspond to *Ec*PrfH. The secondary structures were depicted at the top, and the domain boundaries were marked at the bottom. The triple residues corresponding to the most conserved motifs in RF1 and RF2 are boxed in red.

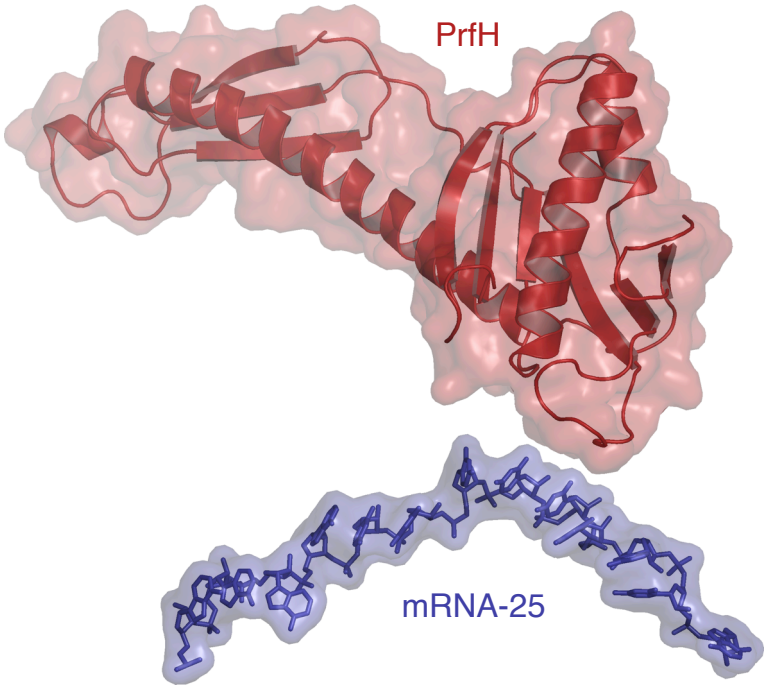

Figure S9. PrfH and mRNA do not make contacts. Structure of the damaged *E. coli* 70S•PrfH•tRNA•mRNA complex. Only the structures of PrfH and mRNA are shown for clarity. PrfH is depicted in cartoon and surface, and mRNA is depicted in sticks and surface. Because there is a gap between the surface representation of these two molecules, we concluded that they are close but do not make contacts.

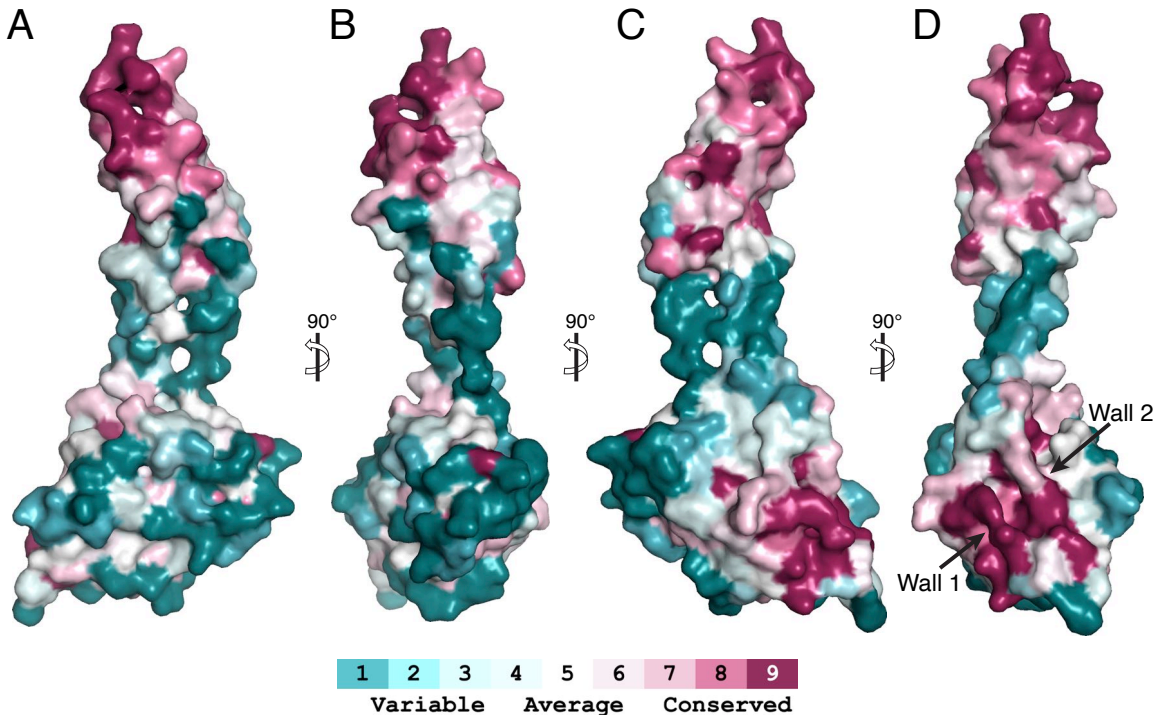

Figure S10. Mapping the conservation of amino acid sequences of PrfH on the structure of *Ec*PrfH. The sequence of *Ec*PrfH and additional 200 randomly selected PrfH sequences were aligned. The aligned PrfH sequences, together with the structure of *Ec*PrfH, were employed for ConSurf analysis, resulting in the conservation of each residue to be assigned a number (1-9). The *Ec*PrfH structure is depicted in surface, with each residue colored by the degree of conservation. The structures in panels *A* and *B* have the same orientation as the ones in Fig. 2*B*. The GGQ domain (top) has the highest conservation, followed by the rRNA-recognition domain (bottom). The linker regions are least conserved. The data shown here are consistent with the sequence alignments displayed in Fig. S8.

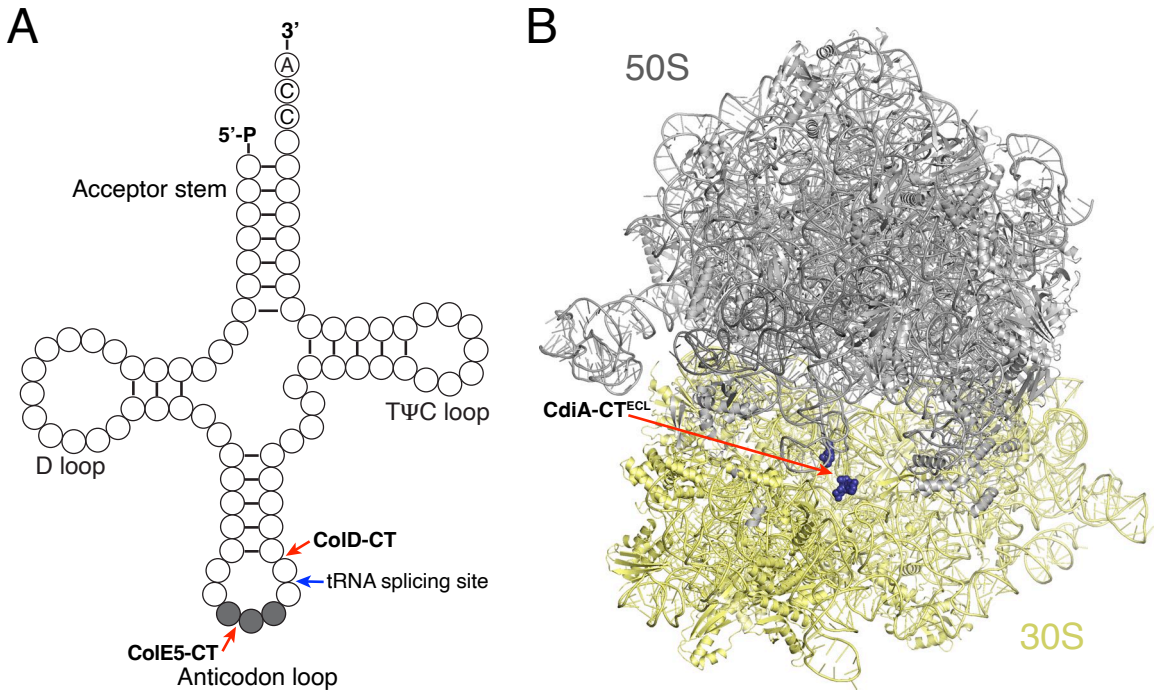

Figure S11. Schematic view of three RNA substrates employed for RNA repair by *Ec*RtcB2 and *Ec*RtcB1. (*A*) Cloverleaf view of tRNA. The anticodons are colored gray. The sites of cleavage by ColE5-CT and ColD-CT are marked with red arrows. The tRNA splicing site, which occurs in archaeal and eukaryotic organisms, is marked with a blue arrow for comparison. (*B*) the cryo-EM structure of the damaged *E. coli* 70S ribosome in complex with PrfH (not shown). The structure is depicted the same as in Fig. 2*A*. The two terminal nucleotides at the cleavage site, A1493P and G1494, are depicted in sphere and colored blue. The conformation of A1493P might be different in the free form of the damaged 70S ribosome.

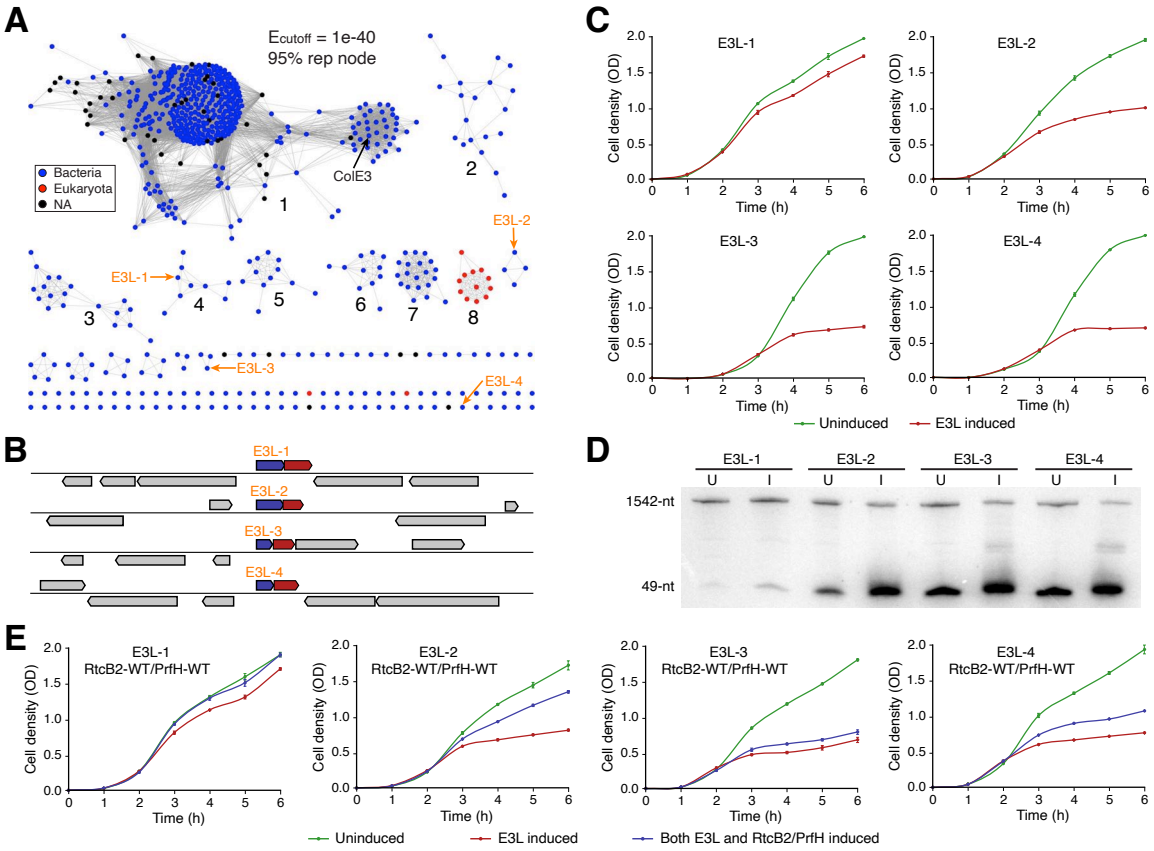

Figure S12. Establishing an in vivo system to evaluate the toxicity of ColE3-like (E3L) ribotoxins, and to investigate *Ec*RtcB2-PrfH neutralizing E3L toxicity in *E. coli* cells. (*A*) SSN of the cytotoxic protein family (Pfam PF09000). ColE3 belongs to this protein family, and its location is marked with a black arrow. Four genes encoding ColE3-like (E3L) ribotoxins, marked with orange arrows, were selected and cloned for our in vivo assays. (*B*) Genomic organizations centered at E3L (colored blue). The neighboring genes (colored red) presumably encode the immunity proteins that inhibit E3L, but they have not been experimentally verified. (*C*) Growth curves of *E. coli* cells without (green) and with (red) the expression of E3L. *E. coli* MG1655 strain was transformed with the pBAD33 plasmid only, which encodes E3L gene. Judged by the extent of inhibition of cell growth, four E3L exhibit different degree of toxicity, with E3L-1 the least toxic, E3L-3/E3L-4 the most toxic, and E3L-2 in between. Each experiment was repeated three times. (*D*) Northern blotting of total RNAs isolated from E3L-expressed cells shown in *C*. The extent of ribosomal damage approximately correlates with the degree of inhibition of cell growth shown in *C*. Ribosomal damage observed from uninduced cells is presumably due to activity of leaked E3L. (*E*) The effect of *Ec*RtcB2-PrfH on the growth of E3L-expressed cells. In addition to the pBAD33 plasmid, *E. coli* MG1655 strain was also transformed with the pQE60 plasmid, which encodes *E. coli rtcB2-prfH* operon. This allows both E3L and RtcB2-PrfH to be expressed simultaneously. Based on the cell growth curves, the efficiency of RtcB2-PrfH neutralizing the toxicity of E3L is in the order of E3L-1 > E3L-2 > E3L-4 > E3L-3. Each experiment was repeated three times.

Table S1. Cryo-EM data collection and model statistics.

	Damaged 70S•PrfH complex
Data Collection	
Particles	997,751
Pixel size (Å)	1.05
Defocus range (μm)	-0.6 to -3.0
Voltage (kV)	300
Electron dose (e^{-}Å^{-2})	30
Model composition	
Non-hydrogen atoms	150,065
Protein residues	6,175
RNA bases	4,724
Ligands (Zn^{2+}/Mg^{2+})	2/439
Refinement	
Resolution (Å)	2.6
$FSC_{average}$	0.90
Rms deviations	
Bond lengths (Å)	0.010
Bond angles (°)	0.843
Validation (proteins)	
MolProbity score	1.81
Clashscore, all atoms	11.31
Favored rotamers (%)	99.37
Ramachandran plot	
Favored (%)	96.34
Outliers (%)	0.05
Validation (RNA)	
Correct sugar puckers (%)	99.51
Good backbone conformations (%)	83.81